CurtainNet: Enabling precise beamforming with a deformable antenna array on a fabric substrate

Xingda Chen, Ankur Aditya, Zhenyu Lei, Deepak Ganesan University of Massachusetts Amherst, Amherst, MA xingdachen,aaditya,zhenyulei@umass.edu,dganesan@cs.umass.edu

ABSTRACT

Recent trends in flexible antennas and printed circuit boards present an opportunity to leverage deformable substrates such as textiles to deploy large UHF, VHF and ISM band antenna arrays in smart homes. Low-frequency large antenna arrays are rarely deployed in indoor settings due to their large size which makes them bulky and difficult to deploy. By embedding these arrays on existing surfaces such as curtains, we can improve through-wall sensing, beamforming for IoT devices equipped with low-power radios and indoor localization of Bluetooth tags.

However, antenna arrays on curtains present new challenges since deformation shifts their phase centers and changes the 3D positions of antennas. We present **CurtainNet**, a flexible UHF-band antenna array on a large surface curtain that leverages a combination of optical and RF tracking to compensate for these changes while dealing with occlusions and phase changes. Results show that **CurtainNet** outperforms alternative methods by more than 155% in beamforming performance and increases indoor range by 20m.

CCS CONCEPTS

• Hardware \rightarrow Beamforming; Digital signal processing; Boardand system-level test; • Networks \rightarrow Wireless access points, base stations and infrastructure.

KEYWORDS

Smart textile, Novel radio network, Beam-forming

ACM Reference Format:

Xingda Chen, Ankur Aditya, Zhenyu Lei, Deepak Ganesan. 2023. Curtain-Net: Enabling precise beamforming with a deformable antenna array on a fabric substrate. In *The 21st ACM Conference on Embedded Networked Sensor Systems (SenSys '23), November 12–17, 2023, Istanbul, Turkiye.* ACM, New York, NY, USA, 13 pages. https://doi.org/10.1145/3625687.3625787

1 INTRODUCTION

The evolution of flexible antennas and flexible printed circuit boards has opened new avenues for embedding wireless antennas onto unconventional substrates. The surge in wearable and mobile devices has fueled this advancement, enabling antennas to be integrated

Permission to make digital or hard copies of all or part of this work for personal or classroom use is granted without fee provided that copies are not made or distributed for profit or commercial advantage and that copies bear this notice and the full citation on the first page. Copyrights for components of this work owned by others than the author(s) must be honored. Abstracting with credit is permitted. To copy otherwise, or republish, to post on servers or to redistribute to lists, requires prior specific permission and/or a fee. Request permissions from permissions@acm.org.

SenSys '23, November 12–17, 2023, Istanbul, Turkiye

© 2023 Copyright held by the owner/author(s). Publication rights licensed to ACM. ACM ISBN 979-8-4007-0414-7/23/11...\$15.00 https://doi.org/10.1145/3625687.3625787

into materials such as paper and textiles [8, 10, 61]. This innovation allows antennas to conform to flexible and curved surfaces, and be installed at arbitrary locations in a building, which expands the design possibilities over conventional rigid phased array elements.

This advancement is particularly beneficial in addressing a key challenge: scaling antenna arrays in lower frequency bands like VHF, UHF, and ISM. In contrast to mmWave antenna arrays, which can compactly fit many elements, low frequency arrays demand a larger footprint. For instance, a 10 by 10 antenna array spans roughly 0.5m x 0.5m at 2.4GHz, but expands to 4.5m x 4.5m at 433MHz. Integrating such arrays onto flexible surfaces like curtains makes them more feasible for indoor applications.

Deploying antenna arrays in the 30MHz to 3GHz range is vital due to the suitability of these frequencies for long-range and energy-efficient communication. Lower frequencies experience less path attenuation compared to higher frequencies, making them optimal for applications requiring long-range or through-wall propagation, such as LoRa [38] and LTE [25]. Moreover, these frequencies offer energy-efficient communication for low-power IoT devices using Bluetooth [37], Zigbee [45], RFID [52], or WiFi HaLow [41].

From an application perspective, low-frequency antenna arrays can significantly enhance communication, sensing, and localization in smart homes. Low frequency beamforming can enable IoT devices to transmit at lower power to reach a base station, saving energy. It can also extend wireless sensing with signals such as LoRa [56, 57], WiFi [12, 40] and LTE [18, 19], providing comprehensive RF-based home security systems, fall detection systems, and occupancy detection coverage. Furthermore, antenna arrays can improve RF localization, expanding the detection range of Bluetooth location tags like Apple AirTags, which currently only have a range of approximately 30 feet.

In this paper, we explore the design challenges when deploying antenna arrays on curtains that are already ubiquitous in homes. Curtains are large and have significant real estate for mounting electronics such as RF front-ends, making them the perfect choice to implement large low-frequency antenna arrays for smart home/IoT environments. In addition, a key advantage of curtains is that installing them does not require any modification to the building or mounting on a wall.

Our work significantly advances the state of the art by building on recent innovations in metamorphic reflector arrays aimed at shaping RF propagation in smart environments[2, 9, 32, 53, 58]. A notable example in this emerging field proposes the utilization of a motorized curtain for beam steering through an antenna array [59]. However, it is essential to underline the substantial differences between this preceding work and our contribution. Previous research mainly concentrates on reflecting RF signals using passive elements, whereas our work tackles active beamforming through antenna

arrays integrated into curtains. This distinction necessitates confronting and addressing an entirely new set of challenges involving the precise orientation and positioning of antennas and their effects on beamforming. Such aspects were not central considerations in previous works.

Challenges: The first challenge involves the variation in phase center of antennas i.e. the point from which the electromagnetic wave effectively appears to emanate. For various antennas, including low-cost ceramic antennas, patch antennas, and flexible antennas, the phase center isn't on the antenna but often offset from it. When these antennas are mounted on a fabric, like a curtain, their orientations vary due to the fabric's folding. Consequently, the phase center offsets can also differ in direction for each antenna. This situation requires meticulous estimation and correction of these offsets to maintain accurate beamforming and signal reception. In contrast to traditional flat antenna arrays, which have uniform phase center offsets that can be pre-calibrated, antennas on fabric substrates like curtains have unpredictable folding. This makes it crucial to employ dynamic methods to account and adjust for phase center offsets.

A second challenge arises from the effect of fabric folding on the positions of the antenna elements. For operations like beamforming to arbitrary angles, it is critical that the relative positions of the antenna elements are known with precision to a fraction of the wavelength. However, unlike in rigid substrates where the distances between elements are fixed, on a fabric, the antenna elements' locations can change dynamically as the fabric folds or stretches. Curtains, for example, can be anywhere between fully extended and completely folded, and this means that the antenna elements' positions can vary widely. Furthermore, these deformations occur in three dimensions, adding another layer of complexity.

Contributions: This paper is a comprehensive empirical exploration of a new design point for wireless communication i.e. beamforming with flexible fabrics. We present **CurtainNet**, a novel, low-cost, curtain-based flexible UHF antenna array that enables effective beamforming in arbitrary directions under day-to-day curtain folding.

With this prototype, we examine how the folding of fabric results in 3D deformations of the antenna array, and how this subsequently impacts the phase centers of the antennas. We demonstrate that such deformations can significantly alter the performance of the array if changes in orientation and position are not adequately compensated for.

We then explore approaches to estimate rotation and position. We show that, in some cases, the combination of visual occlusion and variable orientation necessitates a multi-modal solution. We design a new solution, **CurtainNet**, that jointly localizes antenna elements using both optical and RF-based tracking methods. We leverage the accuracy of the optical tracking system together with the occlusion robustness offered by RF localization to dynamically track the positions and rotation of antenna elements on a curtain subjected to folding.

Our results show that

■ The combination of optical and RF tracking in CurtainNet enables localization of antenna elements under an arbitrary

- folding state and/or under visual occlusions to 1.7–5cm accuracy. In addition, our rotation estimation method has 25° accuracy improvement over alternative methods.
- CurtainNet estimates the incoming signal's direction of arrival (DOA) within 5° error despite folding-induced irregular structure
- The use of **CurtainNet** leads to a gain of over 10*dB* and roughly 20 meter improvement in indoor coverage range compared to alternative solutions.

2 APPLICATIONS & CHALLENGES

Deformable antenna arrays open up new application possibilities and new challenges.

2.1 Applications

Recent work in RF arrays has primarily focused on high-frequency mmWave arrays, with less attention given to large arrays operating in conventional lower-frequency bands (50MHz - 3GHz). This disparity is mainly due to form factor constraints: mmWave antenna arrays can fit into compact spaces, while large arrays composed of low-frequency antennas require significant indoor space, making them cumbersome to deploy.

However, recent advancements in antenna technology, including the integration of novel materials like graphene and conductive polymers, represent a substantial progression in the field. These developments enable embedding of larger, low-frequency antennas in flexible substrates such as curtains, potentially alleviating some challenges associated with traditional low-frequency arrays that required rigid mounting and complicated installation processes.

Utilizing low-frequency antenna arrays enables the exploitation of the band's long-range propagation and obstacle-penetrating characteristics, particularly in indoor settings. For instance, in smart homes, many IoT devices operate in the ISM band, and beamforming can enhance signal reception, reduce interference, and extend range, which is crucial for devices in areas lacking direct line-ofsight communication. Beamforming is also advantageous in RFID systems, as it extends the read range and reliability of RFID tags, especially in environments with tags scattered over a large area or in densely populated tag settings. In industrial automation, beamforming facilitates reliable wireless communication among machines and devices operating predominantly in the lower frequency ISM band, reducing the need for cabling and allowing more adaptable factory layouts. Additionally, wireless audio systems often use low-frequency bands; employing beamforming can precisely direct audio signals to receivers, thereby enhancing audio quality.

2.2 Challenges

Deformation of textile substrates introduces new challenges to the design of antenna arrays. For example, a curtain can be in any configuration between fully expanded and fully folded. This substrate deformation creates unique challenges because the arrays are no longer equally spaced, and the antennas deform with the curtain to bend and orient in different directions. This geometry change would need to be addressed if one wants the array to steer to arbitrary directions where there may not be a dedicated signal source for channel estimation.

Let us examine the deformations that occur on the textile surface when a curtain folds. For arbitrary movement in 3D space, there are position shifts in $\langle x, y, z \rangle$ coordinates, and orientation shifts in $\langle \psi, \theta, \phi \rangle$ angles. A curtain is restricted to folding and expanding along a curtain rod, resulting in a more restrictive set of position and orientation changes on the curtain surface.

Figure 1 demonstrates how a set of antennas change their position and orientation when the curtain folds. We see that there will be a significant position shift along the curtain rod i.e. the horizontal axis y, and the antenna will also displace along the axis perpendicular to the curtain rod z as the curtain cloth folds out of the plane. In terms of orientation, folding results in yawing along the vertical axis when the curtain folds (ϕ in Figure 1).

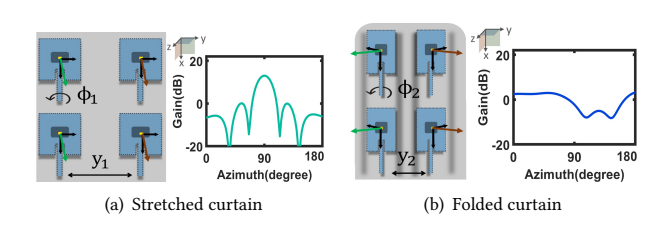


Figure 1: (a) Stretched curtain: Antennas' position and rotation and voltage gain of an 8-element array along the azimuth (yz plane). (b) Folded curtain: Same as before but for a folded curtain.

In this section, we discuss the impact of these changes in antenna geometry on the curtain-embedded antenna array's radiation pattern and hence its beam-forming performance.

2.3 Impact on antenna phase center

The first challenge that folding presents is that the deformation of the fabric changes the orientation of the antenna elements along the folds. The surface curvature of a deformed curtain introduces antenna rotation and bending that is generally not a consideration for conventional rigid antenna arrays since all antennas are flat and move together. But this is not the case for flexible and deformable antenna arrays.

Phase center: To understand how rotation impacts antenna behavior, we have to look at how it impacts the phase center. Every antenna has an imaginary point called the phase center where its spherical wave appears to radiate from. However, the phase center is not necessarily positioned at the geometric center of the antenna, and this position depends on rotation and bending.

Let us look at the phase center for microstrip patch antennas, which are typically low profile and focus their signal toward the front. These antennas are commonly used for integration onto textiles and wearables because they are low-profile and can be designed to be conformal with the underlying substrate.

The phase center of a patch antenna is typically not at the center of the antenna itself but shifted out towards the front by a few centimeters, therefore the rotation of the antenna results in changes in phase front. Commonly used low-cost antennas such as ceramic patch antennas have particularly high phase center variations [54].

To illustrate, we run an antenna EM simulation of a 2.45GHz patch antenna in HFSS to visualize the far-field phase change of the emitted EM wave at equal distances over all azimuth and elevation angles. The simulation results, shown in figure 2(a), indicate that an antenna's phase can vary from -37° to -85° degrees when the antenna is rotated by 60° azimuth.

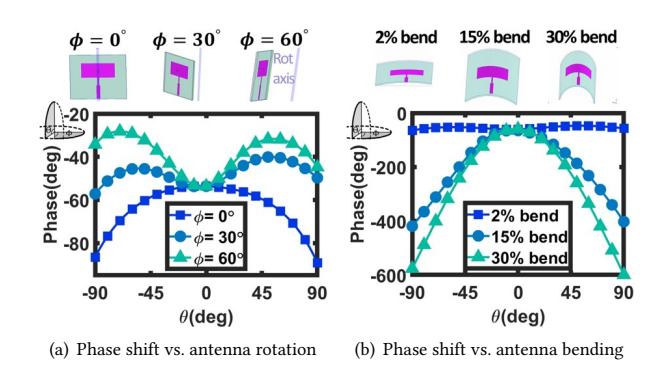


Figure 2: Far-field phase change at equidistant from the patch antenna. (a) Three azimuth rotations -0° , 30° , and 60° . (b) Three degrees of bending -1%, 15%, and 30% (antenna completely folded in half would be 100% bent).

Impact on beamforming: On a curtain, each antenna element will be pointed in a different direction which will result in the phase center offsets of the different antennas being shifted away from their 3D position to different extents. These offsets are difficult to calibrate a priori, hence they need to be handled in an online manner. Typical antenna arrays can ignore these issues since the array is rigid and all antenna elements are oriented in the same direction; hence any phase offset is likely to be the same across all elements.

The fact that different antenna phase centers are offset differently is not an issue if a curtain array only has to transmit back towards the direction of a pilot signal. If a pilot is received from a transmitting source, the curtain array can simply use channel reciprocity to determine optimal weights without requiring knowledge of antenna locations.

However, it is an issue for a broader case where the array needs to actively direct its beam in specific directions, for example, to aid in localizing wireless signals or power delivery.

Loss of gain: How much does rotation-induced phase distortions impact beamforming gain? To answer this question, we ran HFSS simulations on an antenna array with the antennas' rotational motion similar to what we observe in Blender simulations [1] shown in Figure 2(a). This simulation of a 2x4 array with rotation-induced phase shift reveals a gain loss of more than 3dB when half of the elements are rotated for more than 60 degrees, as shown in figure 3(a). The simulation result implies that an eight element array without rotation compensation can only generate the same amount of gain as a four-element array with rotation compensation. The loss in gain will be exacerbated if the antennas are bent in addition to being rotated. Therefore, rotation estimation and compensation

is needed for the antennas embedded on a curtain to retain as much beam-forming power as possible.

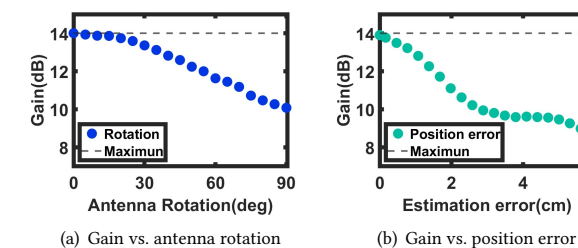


Figure 3: (a) Average gain (voltage) of a 2x4 array with increasing curtain rotation. Maximum gain is when there is no rotation. (b) Gain with increasing positioning error. Maximum gain is obtained when the array is positioned with no location errors.

2.4 Impact on antenna positions

The second challenge is that curtain deformation also changes the location of the antenna elements. Beam-forming from an antenna array towards a direction from which there is no pilot signal requires knowledge of its elements' physical locations. Each antenna element emits a radio wave, so to constructively combine them, we need to apply the appropriate phase shift based on the antennas' physical displacements.

In the case of an antenna array built on a flexible curtain, the displacement depends on the folding state, as shown in Figure 1. When the curtain is completely expanded, the curtain behaves similarly to a traditional rigid antenna array. In this case, the antenna distances are known a priori, and beam-forming weights are computed based on the desired beam-forming angle. When the curtain is folded, the distance between antenna elements changes significantly. Thus, the computation of beam-forming weights at a desired beam-forming angle is inaccurate.

To comprehensively characterize the folding antenna motion and its impact on beam-forming, we simulate a complete curtain folding motion with antenna elements attached using the Blender 3D modeling software. The motion is segmented into 100 frames from the curtain fully closed to fully opened. We export the elements' position and rotation and leverage these data to construct beamforming simulations via MATLAB and HFSS.

The change in the elements' location affects the overall beamforming pattern. Figure 1(a) demonstrates the radiation pattern of a perfectly expanded array at desired beam-forming directions of 0° to 180° azimuth with a set of relevant beam-forming weights computed by a conventional beam-forming algorithm. When using the same weights when the curtain is folded, the beam-forming pattern changes dramatically as shown in figure 1(b), and the gain in the desired direction degrades.

Impact on beamforming: In the case of a traditional regular antenna array, positions are fixed, hence we only need to take into account the beam-forming direction when computing the weights. However, when antenna elements' locations are subjected to 3D

folding in the case of the textile antenna array, the phase delay between adjacent antennas becomes dependent on both beamforming direction and distance between adjacent antennas. Thus, we need to accurately measure the antenna position under the uncertainty of the antenna's rotation.

Loss of gain: How precisely do we need to know the locations of the antennas on the array? To answer this question, let us look at how the precision of antenna localization impacts beamforming gain.

Generally, the level of precision required for localization depends on the RF signal's wavelength. In the ISM band, the wavelength is typically less than 10cm, implying that even a localization error of a few centimeters can significantly impact the performance of array beamforming. Figure 3(b) shows the degradation in beamforming gain of a 2x4 antenna array as the localization error of the antenna element increases. We see that a localization error of more than 4cm results in more than 4dB gain loss. This is quite substantial - a 4dB gain loss means an eight elements array without correct position knowledge can only generate the same amount of gain close to a three-element array with perfect position knowledge. In theory, constructive interference happens when two signals superimpose their waves within a delay of $\frac{2\pi}{3}$, which translates into a localization resolution of around 3cm for a 10 – 12cm wavelength radio. Hence, we need a localization solution that has high precision with error less than a few centimeters.

3 COMPARING TRACKING METHODS

Let us look at how we can estimate rotation and position of each antenna on a curtain. Table 1 compares different technology solutions. IMUs are easy to integrate but are not easy to calibrate; Acoustic can be precise for positioning but requires microphone arrays on the curtain and rotation estimation can be difficult. RF and optical methods are more attractive since they add little complexity to the curtain itself and offloading most of the complexity to infrastructure. From this perspective, we look at how RF and optical methods can achieve our goals.

RF-based positioning: RF-based positioning is better suited for positioning than rotation estimation. Rotation estimation via RF would require having multiple antennas compacting in a small area to approximate the local curvature in sub-centimeter level localization accuracy which will require mmWave frequencies arrays. Given that our focus is on low-frequency arrays, the need for additional high-frequency RF elements would make the hardware more complex, expensive, and power-hungry. Phase-based RF positioning may achieve cm-level resolution if phase center offset can be calibrated but curtain deformation makes this complicated. Thus the canonical RF-based positioning isn't sufficient to precisely determine both rotation and position.

Optical positioning: There are many optical positioning methods that have become popular in recent years. Of these, we focus on "outside-in" methods that use lightweight markers such as LEDs on the object being tracked (in our case the curtain), and rely on infrastructural base stations for tracking.

Both HTC Vive and Oculus Rift are examples of outside-in trackers. Oculus Rift assumes that distance between markers is fixed

	Rotation Estimation	Position Estimation	On-curtain Hardware	Infrastructure
IMU	Low accuracy (due to calibration	Lacks independent localization ca-	Low: IMU per location	None
	issues and drift)	pability		
RF	Cannot estimate rotation of indi-	Limited precision due to ISM	Low: Reuse antenna array	Multiple pilots with known po-
	vidual antenna	Bandwidth and PCO		sitions
Optical	High precision if LoS to optical	High precision if LoS to optical	Low: few photodiodes per	Multiple Optical Base stations
	tracker available.	tracker available.	location	
Acoustic	Challenging due to the nature of	Moderate precision with mic ar-	High: microphone array	Multiple acoustic sources with
	sound propagation.	ray.	per location	known locations

Table 1: Comparative Analysis of Various Technologies for Rotation and Position Estimation

which is not true for us, hence we focus on the HTC Vive "Lighthouse" method.

Optical positioning using Lighthouses only needs a few photodiodes but needs line of sight to the optic sources (base stations)[26, 31, 51, 55]. When the curtain folds, it can occlude the markers from the optic source resulting in situations where only a few antennas can be located by the optical system and the rest do not have a location estimate. Optical trackers like the HTC Vive system address the occlusion problem by using 32 photodiode sensors to position the location of its headset, but it is impractical to incorporate so many photodiode sensors for each antenna in **CurtainNet**.

3.1 Our Idea: Joint Optical-RF Positioning

Our high-level idea is to leverage both RF and Optical positioning to create an accurate tracker of position and orientation. We design **CurtainNet** to be configurable so it works with RF-only or Optical-only positioning methods when the array is flat or visually unobstructed, as well as the more dedicated approach that combines RF and Optical together to address the mentioned issues.

To achieve this, we leverage our observation that optical methods are surprisingly more accurate at estimating orientation than position under rotation. Optical positioning requires that each optical marker can be seen by multiple base stations. However, due to curvature, some markers may be blocked or have low optical sensitivity due to rotation shown in figure 5(a), and the antenna positioning returns a high error. In contrast, we show that orientation estimation is accurate under partial occlusion from base stations, even when there is only one base station visible to the marker.

Thus, our idea is to leverage optical methods as a first-level positioning method which obtains positions of a small number of antennas, as well as the orientation of a majority of antennas. We then use RF methods to fill in the gaps and estimate the positions of the remaining antennas in the array. This allows us to leverage the best of optical and RF methods for positioning and orientation estimation. We describe this procedure in more detail in this paper.

4 CURTAINNET DESIGN

CurtainNet is a configurable curtain-based antenna array platform that can self-calibrate using RF, Optical or a combination of RF and Optical methods to optimize beamforming performance. We describe the hybrid approach involving both optical and RF positioning but evaluate for all configurations. Figure 4 shows a high level pipeline for our system.



Figure 4: CurtainNet pipeline

4.1 Rotation estimation under deformation

In **CurtainNet**, the estimation of an element's rotation is essential to determining the phase center offset, which arises from the rotation or bending of antennas.

Initially, we considered estimating rotation by localizing markers on the curtain using optical localization. This would subsequently aid in determining the orientation. However, we found that the accuracy of optical position estimation was heavily contingent on orientation. If the optical markers were not properly aligned to face the optical tracker, the beams would not be received correctly, causing the location estimation process to fail.

We now present an alternative strategy for discerning board orientation. This approach only necessitates a single Lighthouse base station and does not rely on the precise 3D positions of the diodes.

Optical positioning preliminaries: Our system utilizes a pair of low-power laser emitters as the source, with a set of photodiodes on a custom board acting as markers. The board requires a layout of four photodiodes in a square to initialize and self-calibrate the system. This allows for accurate 3D positioning of the markers [15, 21, 44].

The Light-House (LH) base stations, equipped with pairs of laser emitters and corresponding rotors, form the backbone of the photodiode positioning setup. These base stations emit laser beams that sweep the space both horizontally and vertically at a consistent speed. Prior to each sweep, a synchronization infrared pulse is broadcasted. The onboard Microcontroller Unit (MCU) on the photosensing board records the time difference between the receipt of the broadcasted IR signal and laser beam as clock ticks. Four of these recorded ticks, gathered from two lasers in two base stations, are used to compute the angles of rotor spin. However not all four diodes may receive proper laser beams from both base stations (BS_a and BS_b). For example, under a certain degree of rotation, diode D_1 and D_2 in figure 5(a) may not properly receive laser beam from

base station BS_b . In such case the correct locations of four diodes $(D_1 - D_4)$ is missing thus rotation computation is unattainable or inaccurate.

CurtainNet rotation estimation method involves taking advantage of the fixed relative positions between two vertically stacked diodes, labeled D_0 and D_3 (refer to Figure 5(b)). Based on our observations, a typical day-to-day curtain neither stretches nor folds at the downward direction during folding. Therefore, we can create a trigonometric representation using a single base station to solve for board rotation.

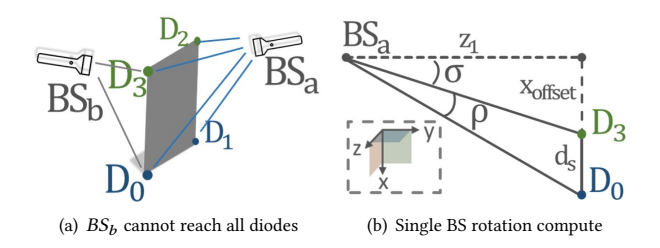


Figure 5: (a) Curvature results in occlusions. (b) Our single BS-based rotation computation.

Let us consider the case where one of the two base stations, BS_a , is visible to the board when the curtain is folded. BS_a is at z_1 distance along the z-axis, d_s is the board size, $\angle \rho$ is the angle sweep by BS_a , which the onboard MCU computes from the received clock ticks, x_{offset} is fixed upon set up, and $\angle \sigma$ is the angle sweep from D_3 to the z-axis parallel. We then solve for z_1 . The same representation is set up for diodes D_1 and D_2 for the distance z_2 , and we can use z_1 and z_2 to determine the board rotation $\angle \phi$. Algorithm 1 summarizes the operation:

Algorithm 1: Compute Board Rotation $\angle \phi$

- 1: Define *x*-axis as downward along curtain
- 2: Define z-axis as outward from curtain to Lighthouse
- Compute z using:
- $\tan\left(\sigma_{1,2}\right) = \frac{x_{\text{offset}}}{z_{1,2}}$
- 5: $\tan (\sigma_{1,2} + \rho_{1,2}) = \frac{x_{\text{offset}} + d_s}{z_{1,2}}$ 6: Compute $\angle \phi$ using: $\angle \phi = \arcsin \frac{z_1 z_2}{d_s}$

A significant advantage of using a single base station for rotation computation is the increased likelihood of at least one photodiode being in the line of sight of a base station's laser beam, even when the curtain is folded. This exposure to a single base station's laser beam occurs far more frequently than simultaneous exposure to the laser beams of multiple base stations. As we'll demonstrate, this approach enables us to estimate rotation even under severe curtain folding. For bendable antennas, since we cannot directly determine the antenna's bending through either optical or RF positioning, we use board rotation as a proxy. The rotation of the board provides a proxy for bending since curtain folding impacts both the curvature and the attached board's rotation simultaneously. Figures 6(a) empirically validates this relationship: we see that board rotation is roughly proportional to the bending angle for the flexible antenna.

In the following section, we will discuss how we integrate this rotation estimation into our model for the antenna's phase center. This integration allows us to calibrate the phase offset caused by folding, which is essential for the computation of the steering vector.

4.2 Estimating the Phase Center Offset

The phase center of an antenna is the modeled reference point from where its signal is assumed to originate. This point often does not coincide with the antenna's geometric center. When the antenna rotates, the phase center displaces along with the rotation. However, this additional phase shift isn't identifiable by the radio receiver, leading to a misinterpretation of the steering vector required to accurately determine relative position, as depicted in Figure 6(b). This deviation between the phase center and the physical center of the antenna, as estimated by an antenna localization method, is referred to as Phase Center Offset (PCO).

To estimate this PCO, we utilize rotation estimations from the optical tracker to approximate the shifts in phase center, denoted as Δx , y, z, relative to the antenna's geometric center for any desired outgoing beam-lobe directions.

Once we have this information, the subsequent step is integrating the estimated PCO into the RF signal model. Specifically, this involves adjusting the phase shifts resulting from the antenna's rotation and bending. Notably, these adjustments cannot be made if using only traditional RF detection.

The modified signal model, accounting for the phase center (referenced as eq2), considers the displacement between the geometric center and the phase center resulting from curtain folding for rigid and flexible antennas. We determine the antenna's phase center location using electromagnetic simulation (HFSS) of a 2.4cm x 2cm geometry patch antenna for both rigid and bent cases from its geometric center. We find that the PCO for a rigid patch is -1.75cm and for a flexible patch is -2cm.

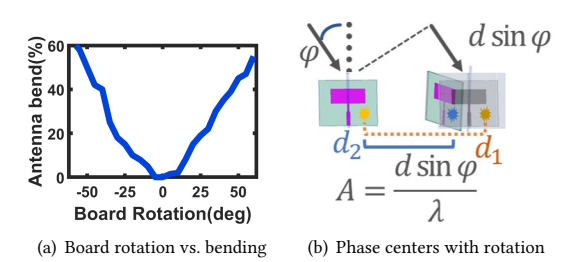


Figure 6: (a) Antenna bending as a function of board rotation on a curtain. (b) The phase center distance is different between a pair of antennas with no rotation and with rotation when the curtain is folded/bent.

4.3 Optical localization of "anchors"

With the Phase Center Offset (PCO) information available for antennas visible to the optical tracker, we can integrate this data into a localization system for curtain arrays. However, there are a few challenges to implement an end-to-end system. As indicated in Table 1, RF-based localization within the ISM band provides low

resolution due to its limited bandwidth and often times required known RF sources' location, while optical-based localization fails under occlusion. Furthermore, optical localization also proves ineffective when a board is heavily rotated relative to the base stations.

To address these issues, we use a two-step approach that utilizes both optical and RF methods. Firstly, we employ optical tracking to localize antennas that are well-oriented towards the optical base stations, which we refer to as "anchors". These anchors, along with the previously obtained PCO estimates, can serve as inputs to an RF-based localization method. This method then calculates positions for the remaining antennas in the array that are either poorly positioned or optically occluded.

Note that if we don't have position data for at least two anchor boards, optical positioning fails, and we default to using RF-only for position estimation. However, practically speaking, we can design the system to ensure that two anchors face the optical tracker by strategically placing them on the upper part of the curtain, which typically folds less than the rest, to ensure they are accurately tracked.

Localizing a photodiode array: The goal is to estimate the location of the antenna, which is offset from the photodiodes. Ideally, the four photodiodes should be arranged in a plane forming a square, with the antenna's center at a fixed distance from them. However, due to estimation variations, the computed positions of the photodiodes don't always form a perfect square and may not lie in the same plane.

To counter this, we use a geometric least squares approach to fit a square in 3D space using the estimated photodiode locations. We then identify the location of the antenna relative to this best-fitted square. Essentially, we minimize the equation ax + by + z + c = 0, where x, y, z represent the estimated positions of the diodes, and a, b, c are scalars that form a fitted plane.

We then calculate the geometric projections of the diodes on this fitted plane and fit these four points into a square using an optimization method[39]. This method aims to find four coordinates that have the least summed distance to the projections, as shown in equation 1.

minimize
$$\sum_{i=1}^{4} ||P_i - P_i'||$$
subject to
$$||P_i - P_{i+1}|| = d_s, i = 1, 2, 3$$

$$(P_2 - P_1) \cdot (P_3 - P_2) = 0$$

$$(P_3 - P_2) \cdot (P_4 - P_3) = 0$$
(1)

Here, we solve for P, representing the positions of the four points that form a square on our estimated plane. P' are the four projections to the plane from the sensed diodes' positions, and d_s is the designed square side length. Finally, we calculate the antenna's location, which is at a fixed offset from P by design.

Which nodes can be chosen as anchors? Choosing the appropriate antennas as anchors greatly impacts beamforming accuracy. We carried out extensive empirical characterization to understand the range of rotations that enable sufficiently accurate antenna positioning with the optical system, as detailed in §6.2. Our studies showed that the localization accuracy remains satisfactory for

antennas rotated within $\pm 10^{\circ} - 20^{\circ}$. Given that rotation information is available to us, we're able to select the boards that are most accurately positioned to serve as anchors.

4.4 Using Opportunistic RF signals

After determining the anchors, we solve for the position of the non-anchor elements using equation 2. To do so, we are required to know the relative phase shifts among each element in an antenna array and the Direction of Arrival (DOA) from the pilots. Essentially, we establish a relationship between the array steering vector from the measured pilot signals and the array geometry, which the info are gathered from both optic and RF sources.

When the optical positioning provides us with location information of a few antennas (at least two), the pilot sources can be placed arbitrarily because it is not necessary to know the location of the pilot sources a priori. This is very useful in practice since we can use already deployed IoT devices as pilot sources without requiring to know their exact position. Our strategy also enables us to circumvent more stringent requirements, such as tight phase/time synchronization across Tx/Rx. Our steps are to first formulate PCO included 3D array model and array steering vector estimation, then estimate the DOA of the pilots, followed by nodes localization and beamforming weights estimation.

PCO included array model and steering vector: The array steering vector delineates the spatial sensitivity of an antenna array to RF signals arriving from varying directions. It's beneficial to consider this vector from a Cartesian perspective, as this step is crucial for merging RF information with optical positional data.

An element in a 3D array has three positional variables [x, y, z] and two directional variables $[\phi, \theta]$ (azimuth and elevation angles). Thus, an n antenna array with 3D position variations and PCO $(\Delta_{x,y,z})$ has the following model:

$$A_{n} = \exp\left(-1j\frac{2\pi(dist'_{x_{n}} + dist'_{y_{n}} + dist'_{z_{n}})}{\lambda}\right)$$

$$dist'_{y} = ysin(\phi)sin(\theta) + \Delta y \sin(\phi) \sin(\theta)$$

$$dist'_{z} = zsin(\theta)cos(\phi) + \Delta z \sin(\theta) \cos(\phi)$$

$$dist'_{x} = xcos(\theta) + \Delta x \cos(\theta)$$
(2)

For array steering vector estimation, let's consider a wireless communication scenario with one transmitting (Tx) source and N receiving (Rx) antennas. The received signal vector of the antenna array, x(t), is given by

$$x(t) = As(t) + n(t) \tag{3}$$

Using this received signal model, we can differentiate the incoming pilot signals into signal space and null space. Reminiscent of the MUSIC algorithm [36], the steering vector of an arbitary recevied antenna array can be found in a vector that minimizes the product with its null subspace \boldsymbol{U}_n as shown below:

$$\begin{array}{ll}
\text{minimize} & A^H(U_n U_n^H)A \\
A
\end{array} \tag{4}$$

It's noteworthy that the minimizing formulation in 4 is independent of the pilot modulation and doesn't require a pilot sequence.

Pilot DOA Estimation: We can now use the estimated phase center displacement for antennas as described in §4.2, Δx , y, z, and the optically tracked anchor positions as described in §4.3, x, y, z, together with the steering vector processed from the pilot signal as described in §4.4, A, to solve for the DOA $[\phi, \theta]$ using equation 2.

Localizing Non-anchor Nodes: After determining the DOA for the pilot, we can compute the locations of the non-anchor nodes on the curtain. Here, we discuss how we search for the steering vector *A* in the objective function 4 using optimization technique to solve the system of equations established in equation 2.

To find the steering vector to compute for the antenna locations (and DOA discussed above), we need to solve the optimization problem (function 4). Although the steering vector and null space eigenvectors may be complex, the product $A^H(U_nU_n^H)A$ is real, and thus, we can minimize function 4 using optimization techniques.

Based on the properties of the steering vector, we set up three constraints that allow us to compute a solution. We omit the consideration of mutual coupling in this formulation as our empirical results suggest that the 3D shifts in positions due to curtain folding, where some adjacent antennas move outwards and inwards, mitigate mutual coupling. Nevertheless, we provide guidelines in Section 7 for integrating mutual coupling into the model if it becomes significant.

Assuming far-field communication, we ensure that all terms in the steering vector have a magnitude of 1, and the real part of the phase shift is always within the interval [-1, 1]. Given these constraints, we reformulate objective function 4 using semi-definite relaxation [7, 33] and arrive at the following optimization formulation 5 that is solvable using standard optimization toolboxes:

minimize
$$\operatorname{trace}((U_nU_n^H)AA^H)$$

subject to $AA^H \geq 0$,
 $\|A_i\| = 1, \ i = 1...n$, (5)
 $\operatorname{Max} \operatorname{Re}(A_i) \leq 1$,
 $\operatorname{Min} \operatorname{Re}(A_i) \geq -1$.

5 IMPLEMENTATION

The key challenge in our implementation was designing a compact and lightweight antenna array to attach to a standard curtain without disturbing its natural folding behavior.

The **CurtainNet** board is shown in Figure 7(a). Our layout includes four photodiodes (BPW-34) in a $2\text{cm} \times 2\text{cm}$ square, positioned 1cm away from the antenna. This design is one of the smallest optical localization boards that use HTC Vive Lighthouse. For the antenna, we use a compact, low profile, and 2.45GHz centered micro-strip patch antenna produced by TAOGLAS (CGIP series). This antenna geometry is run through HFSS and exhibited a phase center offset variation of 2-5cm due to rotation.

We arranged eight elements in a 2×4 pattern on a polyester curtain and ran our evaluation on it. Additionally, we arranged the boards on linen and velvet curtains to demonstrate material versatility (Figure 7(c)). The elements were sparsely separated by 12cm to minimize mutual antenna coupling. The boards were sewn onto the curtain. The whole array is tested in our building floor with optical sources demonstrated in Figure 7(d).

In our experiment, the HTC VIVE Lighthouse base stations were placed 1.2m apart and positioned approximately 3.5m from the curtain. We used tripods to set these up for temporary implementation in one of our office rooms.

Our curtain array, implemented as a receive beamformer, utilizes four USRP X300s [17] at a carrier frequency of 2.45GHz, working concurrently with the aid of OCTO-CLOCK [16]. MATLAB was used to process the raw IQ sample and position data from the photosensing board. Data acquisition, rotation and position estimation, and beamforming algorithms were executed in MATLAB. A pilot transmitter, using an X300 SBX daughterboard, broadcasted the pilot tone from various locations 2m to 12m away from the curtain.





(a) Photo sensing board

(b) Single board test setup





(c) Array setups

(d) Array testing setup

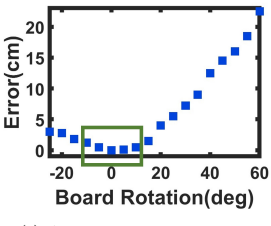
Figure 7: (a) Our photo-sensing board with patch antenna. (b) Single board evaluation using Qualisys system. (c) Array setup on store-bought curtains. (d): Array testing setup in a conference room.

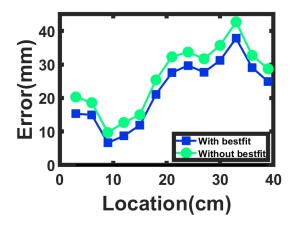
6 EVALUATION

We now evaluate our **CurtainNet** design. We analyze **CurtainNet** at three levels: 1) single board positional and rotational accuracy, 2) RF steering vector estimation accuracy, and 3) combined optical and RF beamforming performance.

6.1 Position estimation validation

We first evaluate the range of rotation for which we achieve sufficiently accurate antenna positioning with the optical system. We compare results from Lighthouse positioning against a commercial Qualisys motion capture system [43]. The photo sensor board is rotated from -25° to 60° to capture the range of rotation during normal curtain usage. Figure 8(a) shows that the error is less than 1.7cm within a $\pm 10^{\circ}$ rotation but increases steadily after that. Figure 8(b) shows the effect of translation of the curtain along the y-axis from 0 to 39cm under 35° x-axis rotation. The best-fit method we use improves accuracy by roughly 5mm, so it can tighten the location estimates and slightly expand the region where optical tracking works by a few additional degrees. The result validates the





(a) Accuracy in various rotation

(b) LH system under test

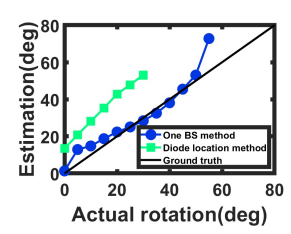
Figure 8: (a) Location accuracy vs. board rotation (avg over 50 measurements for each angle); the photo-sensing board works reliably when the rotation is within 10° . (b) Location estimation of the onboard antenna with and without our best-fit method.

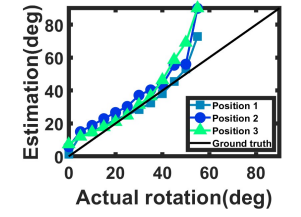
necessity of using rotation estimation to select the most accurately positioned board.

6.2 Rotation estimation verification

We now compare rotation estimation accuracy using the method described in §4.1 against estimation computed directly from diodes' locations. We evaluate this by rotating the board along the x-axis from 0° to 80° with 5° increments (the board position is fixed). Figure 9(a) shows that our method has roughly 25° accuracy improvement which is substantial.

Figure 9(b) shows accuracy at three locations — board close to base station 1, close to base station 2, and close to the center of two base stations. We see that the method is robust and accuracy is similar across all three positions.





(a) Rotation estimation compare

(b) Our method at three locations

Figure 9: (a) Rotation estimation with our method using one BS vs. rotation computed from diode's locations. (b) Rotation estimation is evaluated at three different positions.

6.3 RF subsystem evaluation

Steering vector estimation analysis: We compare our steering vector estimation method against an optical-only baseline that estimates phase shift based solely on antennas that can be localized using the optical tracker and interpolate the rest (in cases where there are too few antennas visible, it assumes that the distance between antennas is the same as the fully extended case i.e. λ).

Figure 10 shows that for the measured pure tone, BASK, BPSK,and BFSK (narrow-band) modulated pilots, **CurtainNet** has phase error less than $\pm 5^{\circ}$. In contrast, the steering vector computed from optically estimated positions has an error that ranges around $\pm 40^{\circ}$ since it often doesn't have enough information.

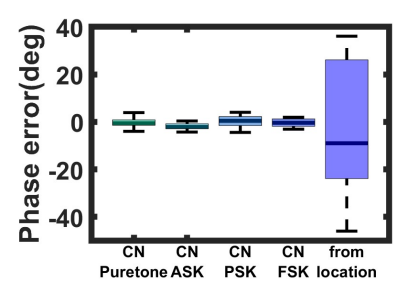
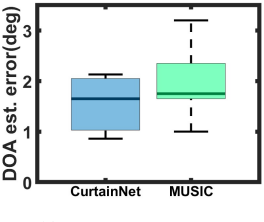
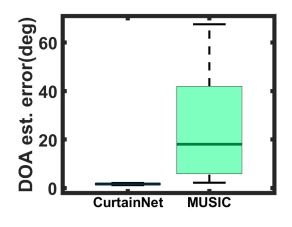


Figure 10: CurtainNet's steering vector estimation evaluated using multiple modulation types vs. an approach using purely Lighthouse-detected locations.

DOA estimation analysis: We now compare the direction of arrival (DOA) estimated using our method against the canonical MUSIC algorithm for 1) a regular linear array configuration with known inter-element distance and 2) an irregular curtain array configuration where only a subset of nodes are visible to the optical tracker. We send these pilot signals from multiple pre-defined angles and estimate our pilot tones' DOA for both configurations.

Figure 11 shows that DOA estimation error is less than 3° for both approaches when the receiving array is linear and distances between elements are known. However, **CurtainNet**'s DOA estimation method outperforms MUSIC when the array is irregular: our error remains under 5° whereas MUSIC has a median error of 20° and third quartile error of more than 40° . Thus, we show that our DOA estimation method is particularly suitable for a deformable curtain array.





(a) Error with linear array

(b) Error with irregular array

Figure 11: (a) DOA estimation between CurtainNet and MU-SIC when the array is linear and positions known. (b) DOA estimation when the array becomes irregular.

6.4 Optical+RF beam-forming performance

CurtainNet can be configured to work in different deployment scenarios where a) Only RF pilots are available, b) Only Optical

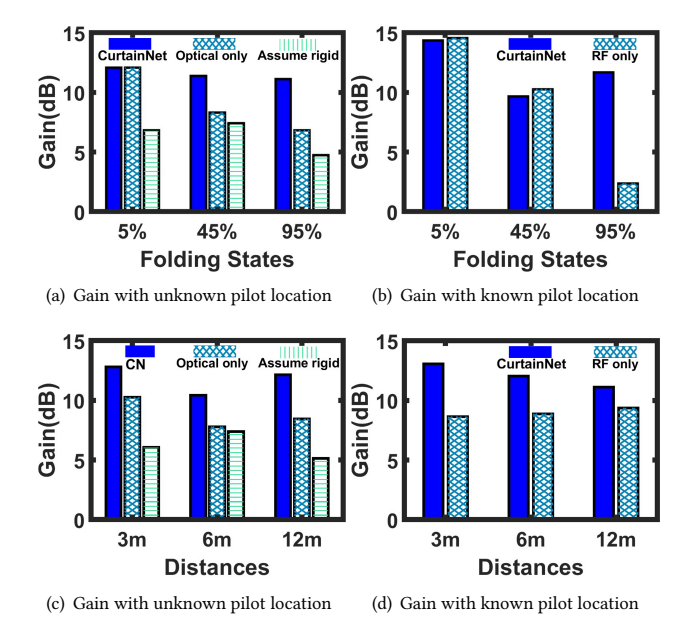


Figure 12: (a), (b): Average beamforming gain from least folded to very folded (5% - 95%). (c), (d): Average beamforming gain from various distances (3m - 12m). Scenarios with unknown and known pilot locations are compared. The curtain array using various localization methods are also evaluated including the comprehensive CurtainNet method.

base stations are available, and c) both Optical base stations and RF pilots are available (with known or unknown RF pilot locations). While our results show that the use of optical + RF has performance advantages in all cases, we focus on one of these in the interest of space.

Beam-forming gain analysis: We look at the case where RF pilot locations are unknown (i.e. arbitrary IoT devices in the home), and we evaluate using assume rigid, Optical-only vs **CurtainNet** methods. We also look at the case where RF pilot locations are known (i.e fixed wireless devices), and we evaluate using RF only vs **CurtainNet** methods.

We place our prototype curtain near a side wall in the room to emulate the real placement of a day-to-day curtain. When the curtain is against the side wall, a $\pm 45^{\circ}$ receiving beam-forming angle can cover most areas in our room. Our curtain array uses these evaluation signals to perform receive beam-forming. To validate the curtain's performance under different folding states and distances, we measure the incoming RF signal under three folding states: 1) little folded (5% fold), 2) regularly folded (45% fold), and 3) completely folded (95% fold). We also validate the performance within three distance ranges for the folds: 1) within 3m, 2) 3m-6m, and 3) more than 12m for a total of 40 test points.

Figure 12 shows the average beam-forming gain of our designed curtain array under five different localization methods. We compute our voltage gain in decibels against the first antenna in our eight elements array.

For the scenario without known pilot locations, we use the 1)**CurtainNet**, 2)optical only and 3)assuming array is rigid methods. As shown in figure 12(a), optical only method delivers an average of $\sim 12.5dB$ gain when the curtain is little folded, and the gain drops to $\sim 8db$ and $\sim 7dB$ when the curtain is regularly folded and completely folded due to the erroneous location estimation from rotation induced visual impairment. **CurtainNet**'s gain starts at $\sim 12.5dB$ and maintained a gain above 11db at all three folding cases. The assume rigid method delivers the poorest result, with average gains on all three folding states under 8dB. For distance comparison, as shown in figure 12(c), **CurtainNet** maintains above 11dB for all tested ranges while other methods are approximately below 10dB.

For the scenario with known pilot locations, we use 1)**Curtain-Net** (without pilot DOA estimation) and RF only methods. As shown in figure 12(b), the RF only method works well when the curtain is little to regularly folded with average gains above 10dB, but the performance significantly drops to $\sim 2dB$ when the curtain is completely folded, which is contributed to the larger distance offset of PCO under heavy rotation. **CurtainNet**'s performance is comparable with the traditional RF only method when the curtain is little and regularly folded, and significantly outperforms in the complete fold state with more than 12dB gain. Figure 12(d) shows that **CurtainNet** is able to maintain above 10.5dB gain at all tested distances and outperforms the RF only method.

For a generic array with flexible substrate, a lighter approach including optical tracking only or RF tracking only delivers decent gain but when the substrate is heavily folded, a combined mode solution such as **CurtainNet** is needed to maintain the performance. Overall, **CurtainNet** outperforms alternative strategies by more than 155% on average in the case of unknown pilot locations. With known pilot locations, it achieves more than 10*dB* gain compare to the alternative when the curtain is heavily folded. Note that a 3*dB* voltage gain to an 8-element antenna array is approximately equivalent to using a 12-element array at 0*dB* gain.

CurtainNet's indoor coverage performance: We now look at the benefits of using **CurtainNet** for possible indoor transmit signal coverage. We estimate the RF strength using our curtain array in our office floor, which is around 90*m* by 45*m* and consists of 20 conference rooms separated by concrete dry walls. We use the mean gain from the test points and a typical 6*dB* loss [46] for these office walls and employ the Motley-Keenan propagation model [23] to compute the path loss in the indoor environment [22]. Figure 13 shows coverage using **CurtainNet** versus the optical-only method. We see that there is roughly a 20*m* range difference between the methods.

7 DISCUSSION

In our design of **CurtainNet**, we have encountered several roadblocks and opportunities for future work.

Towards infrastructure-less integration: We currently deploy a set of optical trackers within visible range of the curtain. To further reduce tracking infrastructure, the base stations can be installed at a more permanent location such as the ceiling. To enable infrastructure-less localization, we are exploring new approaches including the use of optical threads (e.g., [20, 42]) to detect surface

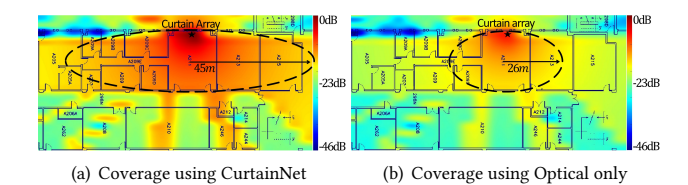


Figure 13: Through-wall coverage at our office building using CurtainNet.

bending, magnetic sensors for localization [5, 24], and ML-assisted methods that fuse information from vision and RF.

Towards fully flexible CurtainNet: In principle, our design can be made fully flexible with flexible PCBs, woven antennas, and flexible interconnects. This is a substantial engineering challenge from a mechanical design perspective and requires custom-optimized elements such as woven antennas that are unavailable in the market. Our immediate intended effort towards full flexible CurtainNet is to develop customized flexible antennas with compatible PCB and antenna substrates and seamlessly integrate them with tailer interconnects.

Array mutual coupling correction: We do not specifically tackle mutual coupling effects among antennas in this work since we find that the 3D movement of the antenna elements tends to reduce coupling. We note, however, that the received signal model in equation 3 can be generalized to include the squared mutual coupling matrix (MCM),C and the mutual coupling compensation matrix (MCCM) C^{-1} to compensate for the impact of elemental-wise coupling if one chooses to design a closely spaced array on a curtain [27, 48]: $x(t) = C^{-1}CAs(t) + n(t)$.

Massive beam-forming applications: In this study, we developed a prototype featuring an 8-element array to conduct far-field beam-forming. As VHF/UHF arrays evolve in scale, we are exploring novel end-to-end IoT applications, including high-power, far-field RF node energy harvesting. The capabilities of the flexible substrates permit a node count significantly exceeding 8, thereby amplifying RF gain. As we scale the array, a nascent area of investigation involves operating within the near-field regime, including the formulation of near-field signal models for deformable arrays.

8 RELATED WORK

We briefly review related work that has not been highlighted.

Improving indoor RF coverage with large arrays: Several recent efforts have explored the deployment of large antenna arrays with meta-surfaces to improve indoor coverage. Closest to our work is the idea of metamorphic surfaces [59], which is a motorized curtain that actively moves to steer the beam. Scrolls[35] investigate the radiating frequencies of metal wires under surface bending. RF-Mediator[34] controls the metallic patterns on a flexible surface to achieve medium virtualization. We look at enabling beamforming via antenna arrays on normally used curtains that are folded during use. Smart-walls such as mmWall, LLaMA, LAIA, RFocus e.g[2, 3, 9, 13, 29, 30, 32, 53, 58] boost coverage by designing a wall with meta-surfaces or RF switches that redirect waves towards desired locations. These are also intended for large surfaces

like ours but focus on rigid non-foldable arrays. LAVA [60] is an ad-hoc array network that uses a number of amplifiers that also intends to improve coverage but focuses on improving multi-hop relay connections.

Irregular antenna array development: There has been mostly theoretical work on the study of irregular antenna arrays [14] [11][4]. These efforts analyze complex signal models and develop computational algorithms that help estimate channel state information (CSI) using generic irregularly placed antenna array [14] [11][4]. CurtainNet is a specialized experimental solution that includes a hybrid optical-RF location/rotation tracker and a signal model specifically designed to address fabric curvature.

Indoor localization: There is a substantial body of work on indoor localization via optical tracking (e.g. VR systems [6, 31]; self-driving cars [26, 51] and robotics systems [21, 44, 55]) and ISM band RF-based locationing (SpotFi[28], Chronos[49], Shirehjini et al. [47] and others). While RF can bypass optical occlusions and its localization technologies and offer roughly 10cm localization performance, consistently achieving 1-2cm accuracy is more difficult and usually requires additional use case requirements (for example, RF-compass[50] achieves *cm* level accuracy but requires continuous motion from a robot). **CurtainNet** leverages optic-based and RF-based approaches to achieve this despite occlusions and deformations to enable precise beamforming on fabric.

9 CONCLUSIONS

In this paper, we argue that fabric substrates present a promising new opportunity for deploying large-size low-frequency antenna arrays in built environments like homes, offices, and schools. Our work explores the challenges posed by these deformable antenna arrays that result in curtain curvature and induce antenna rotation and bending. We present a hybrid tracking solution for the continuous positioning of array elements using low-cost optical trackers and RF anchors. We show that ${\bf CurtainNet}$ achieves more than 12db beamforming gain and roughly 20m increase in coverage radius. Our work opens up new directions in fabric-based wireless antenna arrays, and has several applications including indoor localization, beamforming, through-wall sensing, and long-range remote communication.

10 ACKNOWLEDGEMENTS

This work was funded by the National Science Foundation under agreement CSR Medium 1763524. We also acknowledge support from the National Science Foundation under agreements 1815347 and 1839999.

REFERENCES

- [1] Blender. https://www.blender.org/. [Online; accessed 13-Feb-2023].
- [2] A steerable, transflective metamaterial surface for NextG mmWave networks. In 20th USENIX Symposium on Networked Systems Design and Implementation (NSDI 23), Boston, MA, Apr. 2023. USENIX Association.
- [3] V. Arun and H. Balakrishnan. RFocus: Beamforming using thousands of passive antennas. In 17th USENIX Symposium on Networked Systems Design and Implementation (NSDI 20), pages 1047–1061, Santa Clara, CA, Feb. 2020. USENIX Association.
- [4] C. Bencivenni, M. Coldrey, R. Maaskant, and M. V. Ivashina. Aperiodic switched array for line-of-sight mimo backhauling. *IEEE Antennas and Wireless Propagation Letters*, 17(9):1712–1716, 2018.
- [5] S. Bian, B. Zhou, H. Bello, and P. Lukowicz. A wearable magnetic field based proximity sensing system for monitoring covid-19 social distancing. In *Proceedings of the 2020 ACM International Symposium on Wearable Computers*, ISWC '20, page 22–26, New York, NY, USA, 2020. Association for Computing Machinery.
- [6] M. Borges, A. Symington, B. Coltin, T. Smith, and R. Ventura. Htc vive: Analysis and accuracy improvement. In 2018 IEEE/RSJ International Conference on Intelligent Robots and Systems (IROS), pages 2610–2615, 2018.
- [7] S. Boyd and L. Vandenberghe. Convex Optimization. Cambridge University Press, Cambridge, UK, 2004.
- [8] L. Buechley, D. Mellis, H. Perner-Wilson, E. Lovell, and B. Kaufmann. Living wall: programmable wallpaper for interactive spaces. In *Proceedings of the 18th ACM international conference on Multimedia*, pages 1401–1402, 2010.
- [9] L. Chen, W. Hu, K. Jamieson, X. Chen, D. Fang, and J. Gummeson. Pushing the physical limits of iot devices with programmable metasurfaces. In NSDI, pages 425–438, 2021.
- [10] X. Chen, D. Ganesan, J. Gummeson, and M. Rostami. Cocoon: A conductive substrate-based coupled oscillator network for wireless communication. In Proceedings of the 19th ACM Conference on Embedded Networked Sensor Systems, SenSys '21, page 84–96, New York, NY, USA, 2021. Association for Computing Machinery.
- [11] L. Cheng, C. Xing, and Y.-C. Wu. Irregular array manifold aided channel estimation in massive mimo communications. *IEEE Journal of Selected Topics in Signal Processing*, 13(5):974–988, 2019.
- [12] K. Chetty, G. E. Smith, and K. Woodbridge. Through-the-wall sensing of personnel using passive bistatic wifi radar at standoff distances. *IEEE Transactions on Geoscience and Remote Sensing*, 50(4):1218–1226, 2012.
- [13] K. W. Cho, Y. Ghasempour, and K. Jamieson. Towards dual-band reconfigurable metasurfaces for satellite networking. In Proceedings of the 21st ACM Workshop on Hot Topics in Networks, HotNets '22, page 17–23, New York, NY, USA, 2022. Association for Computing Machinery.
- [14] W. Dong, Z.-H. Xu, X.-H. Liu, L.-S.-B. Wang, and S.-P. Xiao. Modular subarrayed phased-array design by means of iterative convex relaxation optimization. *IEEE Antennas and Wireless Propagation Letters*, 18(3):447–451, 2019.
- [15] esar. Vivepos. https://github.com/esar/vivepos, 2021.
- [16] a. N. I. C. Ettus Research. Octoclock. https://www.ettus.com/all-products/ octoclock/, 2021.
- [17] a. N. I. C. Ettus Research. X300 kit. https://www.ettus.com/all-products/x300-kit/, 2021.
- [18] Y. Feng, Y. Xie, D. Ganesan, and J. Xiong. Lte-based pervasive sensing across indoor and outdoor. In *Proceedings of the 19th ACM Conference on Embedded Networked Sensor Systems*, SenSys '21, page 138–151, New York, NY, USA, 2021. Association for Computing Machinery.
- [19] Y. Feng, Y. Xie, D. Ganesan, and J. Xiong. Lte-based low-cost and low-power soil moisture sensing. In *Proceedings of the 20th ACM Conference on Embedded Networked Sensor Systems*, SenSys '22, page 421–434, New York, NY, USA, 2023. Association for Computing Machinery.
- [20] P. Ferraro and G. De Natale. On the possible use of optical fiber bragg gratings as strain sensors for geodynamical monitoring. Optics and Lasers in Engineering, 37(2-3):115-130, 2002.
- [21] W. Giernacki, M. Skwierczyński, W. Witwicki, P. Wroński, and P. Kozierski. Crazyflie 2.0 quadrotor as a platform for research and education in robotics and control engineering. In 2017 22nd International Conference on Methods and Models in Automation and Robotics (MMAR), pages 37–42, 2017.
- [22] S. Hosseinzadeh. Multi wall (cost231) signal propagation models + python code. https://www.mathworks.com/matlabcentral/fileexchange/61340-multiwall-cost231-signal-propagation-models-python-code, 2023. Accessed February 15, 2023.
- [23] S. Hosseinzadeh, H. Larijani, and K. Curtis. An enhanced modified multi wall propagation model. 2017 Global Internet of Things Summit (GIoTS), pages 1–4, 2017.
- [24] M. A. Ibrahim, G. Hassan, K. Monea, H. S. Hassanein, and K. Obaia. A ferrous-selective proximity sensor for industrial internet of things. In ICC 2020 2020 IEEE International Conference on Communications (ICC), pages 1–6, 2020.
- [25] S. Kanchi, S. Sandilya, D. Bhosale, A. Pitkar, and M. Gondhalekar. Overview of lte-a technology. In 2013 IEEE Global High Tech Congress on Electronics, pages

- 195-200 2013
- [26] F. Kendoul, I. Fantoni, and K. Nonami. Optic flow-based vision system for autonomous 3d localization and control of small aerial vehicles. *Robotics and Autonomous Systems*, 57(6-7):591–602, 2009.
- [27] D.-W. Kim and S. Nam. Mutual coupling compensation in receive-mode antenna array based on characteristic mode analysis. *IEEE Transactions on Antennas and Propagation*, 66(12):7434–7438, 2018.
- [28] M. Kotaru, K. Joshi, D. Bharadia, and S. Katti. Spotfi: Decimeter level localization using wifi. In Proceedings of the 2015 ACM Conference on Special Interest Group on Data Communication, SIGCOMM '15, page 269–282, New York, NY, USA, 2015. Association for Computing Machinery.
- [29] G. Lan, M. F. Imani, P. d. Hougne, W. Hu, D. R. Smith, and M. Gorlatova. Wireless sensing using dynamic metasurface antennas: Challenges and opportunities. *IEEE Communications Magazine*, 58(6):66–71, 2020.
- [30] G. Lan, M. F. Imani, Z. Liu, J. Manjarrés, W. Hu, A. S. Lan, D. R. Smith, and M. Gorlatova. Metasense: Boosting rf sensing accuracy using dynamic metasurface antenna. *IEEE Internet of Things Journal*, 8(18):14110–14126, 2021.
- [31] S. M. LaValle, A. Yershova, M. Katsev, and M. Antonov. Head tracking for the oculus rift. In 2014 IEEE International Conference on Robotics and Automation (ICRA), pages 187–194, 2014.
- [32] Z. Li, Y. Xie, L. Shangguan, R. I. Zelaya, J. Gummeson, W. Hu, and K. Jamieson. Towards programming the radio environment with large arrays of inexpensive antennas. In NSDI, 2019.
- [33] Z.-q. Luo, W.-k. Ma, A. M.-c. So, Y. Ye, and S. Zhang. Semidefinite relaxation of quadratic optimization problems. *IEEE Signal Processing Magazine*, 27(3):20–34, 2010.
- [34] R. Ma and W. Hu. Cross-media wireless made easier: Tuning media interfaces with flexible metasurfaces. 2023.
- [35] R. Ma, W. Hu, and R. I. Zelaya. Softly, deftly, scrolls unfurl their splendor: Rolling flexible surfaces for wideband wireless. MobiCom '23. Association for Computing Machinery, 2023.
- [36] MathWorks. Music super-resolution doa estimation. https://www.mathworks. com/help/phased/ug/music-super-resolution-doa-estimation.html, 2021.
- [37] K. Morsi, X. Huagang, and G. Qiang. Performance estimation and evaluation of bluetooth frequency hopping selection kernel. In 2009 Joint Conferences on Pervasive Computing (ICPC), pages 461–466, 2009.
- Pervasive Computing (JCPC), pages 461–466, 2009.
 [38] U. Noreen, A. Bounceur, and L. Clavier. A study of lora low power and wide area network technology. In 2017 International Conference on Advanced Technologies for Signal and Image Processing (ATSIP), pages 1–6, 2017.
- [39] U. on Stack Overflow. Find the pair of closest points from two sets of points. https://stackoverflow.com/a/9632444. 2011.
- [40] J. Purat, N. J. Lehmann, M. Karagulle, and A. Voisard. Halownet a wifi halow network-based information system for the provision of multi-sided applications for medical emergency scenarios. In 2022 IEEE 10th International Conference on Healthcare Informatics (ICHI), pages 519–521, Los Alamitos, CA, USA, jun 2022. IEEE Computer Society.
- [41] L. Qiao, Z. Zheng, W. Cui, and L. Wang. A survey on wi-fi halow technology for internet of things. In 2018 2nd IEEE Conference on Energy Internet and Energy System Integration (EI2), pages 1–5, 2018.
- [42] H. Qu, T. Brastaviceanu, F. Bergeron, J. Olesik, I. Pavlov, T. Ishigure, and M. Skorobogativ. Photonic bandgap bragg fiber sensors for bending/displacement detection. Appl. Opt., 52(25):6344-6349, Sep 2013.
- [43] Qualisys. Human biomechanics and sports research. https://www.qualisys.com/ life-sciences/human-biomechanics-and-sports-research/, accessed 2023-02-15.
- [44] D. Quiñones, G. Lopes, D. Kim, C. Honnet, D. Moratal, and A. Kampff. HIVE Tracker: a tiny, low-cost, and scalable device for sub-millimetric 3D positioning. In Augmented Human International Conference, Seoul, South Korea, Feb. 2018.
- [45] C. M. Ramya, M. Shanmugaraj, and R. Prabakaran. Study on zigbee technology. In 2011 3rd International Conference on Electronics Computer Technology, volume 6, pages 297–301, 2011.
- [46] T. R. Rao and D. Balachander. Rf propagation investigations at 915/2400 mhz in indoor corridor environments for wireless sensor communications. Progress in Electromagnetics Research B, 47:359–381, 2013.
- [47] A. A. N. Shirehjini, A. Yassine, and S. Shirmohammadi. An rfid-based position and orientation measurement system for mobile objects in intelligent environments. IEEE Transactions on Instrumentation and Measurement, 61(6):1664–1675, 2012.
- [48] H. Singh, S. H L, and R. Jha. Mutual coupling in phased arrays: A review. International Journal of Antennas and Propagation, 2013, 01 2013.
- [49] D. Vasisht, S. Kumar, and D. Katabi. Decimeter-level localization with a single wifi access point. In 13th {USENIX} Symposium on Networked Systems Design and Implementation ({NSDI} 16), pages 165–178, 2016.
- [50] J. Wang, F. Adib, R. Knepper, D. Katabi, and D. Rus. Rf-compass: Robot object manipulation using rfids. In Proceedings of the 19th Annual International Conference on Mobile Computing Networking, MobiCom '13, page 3–14, New York, NY, USA, 2013. Association for Computing Machinery.
- [51] J. Wang and Y. Takahashi. Indoor mobile robot self-localization based on a low-cost light system with a novel emitter arrangement. Robomech J, 5:17, 2018.

- [52] R. Want. An introduction to rfid technology. IEEE Pervasive Computing, 5(1):25– 33, 2006
- [53] A. Welkie, L. Shangguan, J. Gummeson, W. Hu, and K. Jamieson. Programmable radio environments for smart spaces. In *Proceedings of the 16th ACM Workshop* on Hot Topics in Networks, HotNets-XVI, page 36–42, New York, NY, USA, 2017. Association for Computing Machinery.
- [54] D. Willi, M. Meindl, H. Xu, and M. Rothacher. Gnss antenna phase center variation calibration for attitude determination on short baselines. *Navigation: Journal of The Institute of Navigation*, 65(4):643–654, 2018.
- [55] X. Xiao, Y. Fan, J. Dufek, and R. Murphy. Indoor uav localization using a tether. In 2018 IEEE International Symposium on Safety, Security, and Rescue Robotics (SSRR), pages 1–6, 2018.
- [56] B. Xie, D. Ganesan, and J. Xiong. Embracing lora sensing with device mobility. In 20th ACM Conference on Embedded Networked Sensor Systems (SenSys), pages 349–361. ACM, 2022.
- [57] B. Xie and J. Xiong. Combating interference for long range lora sensing. In 18th ACM Conference on Embedded Networked Sensor Systems (SenSys), pages 69–81.

- ACM, 2020.
- [58] R. I. Zelaya, R. Ma, and W. Hu. Towards 6g and beyond: Smarten everything with metamorphic surfaces. In *Proceedings of the Twentieth ACM Workshop on Hot Topics in Networks*, HotNets '21, page 155–162, New York, NY, USA, 2021. Association for Computing Machinery.
- [59] R. I. Zelaya, R. Ma, and W. Hu. Towards 6g and beyond: Smarten everything with metamorphic surfaces. In *Proceedings of the Twentieth ACM Workshop on Hot Topics in Networks*, HotNets '21, page 155–162, New York, NY, USA, 2021. Association for Computing Machinery.
- [60] R. I. Zelaya, W. Sussman, J. Gummeson, K. Jamieson, and W. Hu. Lava: Fine-grained 3d indoor wireless coverage for small iot devices. In *Proceedings of the 2021 ACM SIGCOMM 2021 Conference*, SIGCOMM '21, page 123–136, New York, NY, USA, 2021. Association for Computing Machinery.
- [61] Y. Zhang, C. Yang, S. E. Hudson, C. Harrison, and A. Sample. Wall++ room-scale interactive and context-aware sensing. In Proceedings of the 2018 CHI Conference on Human Factors in Computing Systems, pages 1–15, 2018.